We are IntechOpen, the world's leading publisher of Open Access books Built by scientists, for scientists

4,800
Open access books available

122,000
International authors and editors

135M
Downloads

Our authors are among the

154
Countries delivered to

TOP 1%
most cited scientists

12.2%
Contributors from top 500 universities

CLARIVATE ANALYTICS BOOK CITATION INDEX INDEXED

WEB OF SCIENCE™

Selection of our books indexed in the Book Citation Index in Web of Science™ Core Collection (BKCI)

Interested in publishing with us?
Contact book.department@intechopen.com

Numbers displayed above are based on latest data collected.
For more information visit www.intechopen.com

2

Linearization of radial force characteristic of active magnetic bearings using finite element method and differential evolution

Boštjan Polajžer, Gorazd Štumberger, Jože Ritonja and Drago Dolinar
University of Maribor, Faculty of Electrical Engineering and Computer Science
Slovenia

1. Introduction

Active magnetic bearings (AMBs) are used to provide contact-less suspension of a rotor (Schweitzer et al., 1994). No friction, no lubrication, precise position control, and vibration damping make AMBs appropriate for different applications. In-depth debate about the research and development has been taken place the last two decades throughout the magnetic bearings community (ISMB12, 2010). However, in the future it is likely to be focused towards the superconducting applications of magnetic bearings (Rosner, 2001). Nevertheless, the discussion in this work is restricted to the design and analysis of "classical" AMBs, which are indispensable elements for high-speed, high-precision machine tools (Larsonneur, 1994). Two radial AMBs, which control the vertical and horizontal rotor displacements in four degrees of freedom (DOFs) are placed at the each end of the rotor, whereas an axial AMB is used to control the fifth DOF, as it is shown in Fig. 1. Rotation (the sixth DOF) is controlled by an independent driving motor. Because AMBs constitute an inherently unstable system, a closed-loop control is required to stabilize the rotor position. Different control techniques (Knospe & Collins, 1996) are employed to achieve advanced features of AMB systems, such as higher operating speeds or control of the unbalance response. However, a decentralized PID feedback is, even nowadays, normally used in AMB industrial applications, whereas prior to a decade ago, more than 90% of the AMB systems were based on PID decentralized control (Bleuer et al., 1994).

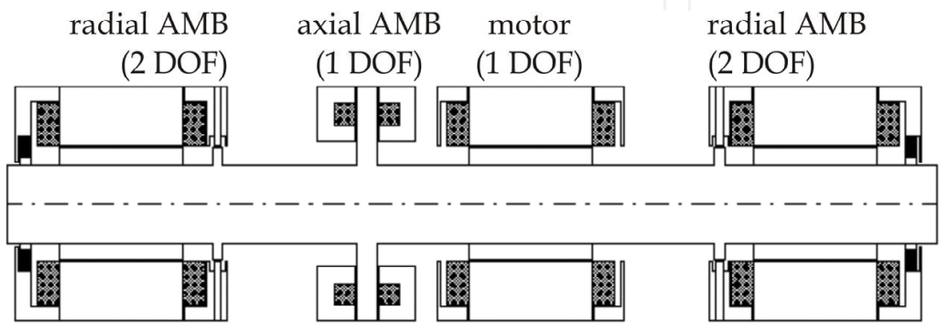

Fig. 1. Typical AMB system

The development and design of AMBs is a complex process, where possible interdependencies of requirements and constrains should be considered. This can be done either by trials using analytical approach (Maslen, 1997), or by applying numerical optimization methods (Meeker, 1996; Carlson-Skalak et al., 1999; Štumberger et al., 2000). AMBs are a typical non-linear electro-magneto-mechanical coupled system. A combination of stochastic search methods and analysis based on the finite element method (FEM) is recommended for the optimization of such constrained, non-linear electromagnetic systems (Hameyer & Belmans, 1999).

In this work the numerical optimization of radial AMBs is performed using differential evolution (DE) – a direct search algorithm (Price et al., 2005) – and the FEM (Pahner et al., 1998). The objective of the optimization is to linearize current and position dependent radial force characteristic over the entire operating range. The objective function is evaluated by two dimensional FEM-based magnetostatic computations, whereas the radial force is determined using Maxwell's stress tensor method. Furthermore, through the comparison of the non-optimized and optimized radial AMB, the impact of non-linearities of the radial force characteristic, on static and dynamic properties of the overall system is evaluated over the entire operating range.

2. Radial Force Characteristic of Active Magnetic Bearings

An eight-pole radial AMB is discussed, as it is shown in Fig. 2. The windings of all electromagnets are supplied in such a way, that a NS-SN-NS-SN pole arrangement is achieved. Four independent magnetic circuits – electromagnets are obtained in such way. The electromagnets in the same axis generate the attraction forces acting on the rotor in opposite directions. The resultant radial force of such a pair of electromagnets is a non-linear function of the currents, rotor position, and magnetization of the iron core. The differential driving mode of currents is introduced by the following definitions: $i_1 = I_0 + i_x$, $i_2 = I_0 - i_x$, $i_3 = I_0 + i_y$, and $i_4 = I_0 - i_y$, where I_0 is the constant bias current, i_x and i_y are the control currents in the x and y axis, where $| i_x | \leq I_0$, and $| i_y | \leq I_0$.

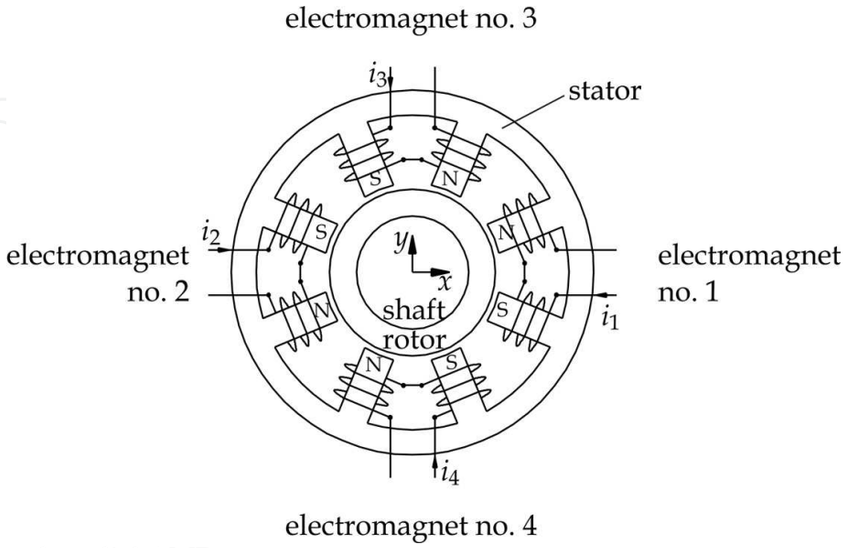

Fig. 2. Eight-pole radial AMB

2.1 Linearized AMB model for one axis

When the magnetic non-linearities and cross-coupling effects are neglected, the force generated by a pair of electromagnets in the x axis can be expressed by (1). δ_0 is the nominal air gap for the rotor central position ($x = y = 0$), μ_0 is permeability of vacuum, N is the number of turns of each coil, and A is the area of one pole. Note that the force generated by a pair of electromagnets in the y axis is defined in the same way as in (1).

$$F_x = \frac{1}{4}\mu_0 A N^2 \cos(\pi/8)\left(\left(\frac{I_0 + i_x}{\delta_0 - x}\right)^2 - \left(\frac{I_0 - i_x}{\delta_0 + x}\right)^2\right) \tag{1}$$

Non-linear equation (1) can be linearized at a nominal operating point ($x = 0$, $i_x = 0$). The obtained linear equation (2) is valid only in the vicinity of the point of linearization. In such way two parameters are introduced at a nominal operating point; the current gain $h_{x,\mathrm{nom}}$ by (3) and the position stiffness $c_{x,\mathrm{nom}}$ by (4).

$$F_x = h_{x,\mathrm{nom}}\, i_x + c_{x,\mathrm{nom}}\, x \tag{2}$$

$$h_{x,\mathrm{nom}} = \left.\frac{\partial F_x}{\partial i_x}\right|_{(i_x=0,x=0)} = \mu_0 A N^2 \cos(\pi/8)\,\frac{I_0}{\delta_0^2} \tag{3}$$

$$c_{x,\mathrm{nom}} = \left.\frac{\partial F_x}{\partial x}\right|_{(i_x=0,x=0)} = \mu_0 A N^2 \cos(\pi/8)\,\frac{I_0^2}{\delta_0^3} \tag{4}$$

The motion of the rotor between two electromagnets in the x axis is described by (5), where m is the mass of the rotor. When the equation (2) is used then the linearized AMB model for one axis is described by (6).

$$F_x = m\frac{d^2x}{dt^2} \tag{5}$$

$$\frac{d^2x}{dt^2} = \frac{h_{x,\mathrm{nom}}}{m} i_x + \frac{c_{x,\mathrm{nom}}}{m} x \tag{6}$$

The dynamic model (6) is used for determining the controller settings, where the nominal values of the model parameters are used ($h_{x,\mathrm{nom}}$ and $c_{y,\mathrm{nom}}$). However, due to the magnetic non-linearities, the current gain and position stiffness vary according to the operating point. Consequently, a damping and stiffness of the closed-loop system might be deteriorated in the cases of high signal amplitudes, such as heavy load unbalanced operation.

2.2 Magnetic field distribution and radial force computation using FEM

The magnetostatic problem is formulated by Poisson's equation (7), where **A** denotes the magnetic vector potential, ν is the magnetic reluctivity, **J** is the current density, • denotes the dot product and ∇ is the Hamilton's differential operator.

$$\nabla \bullet (\nu \nabla \mathbf{A}) = -\mathbf{J} \tag{7}$$

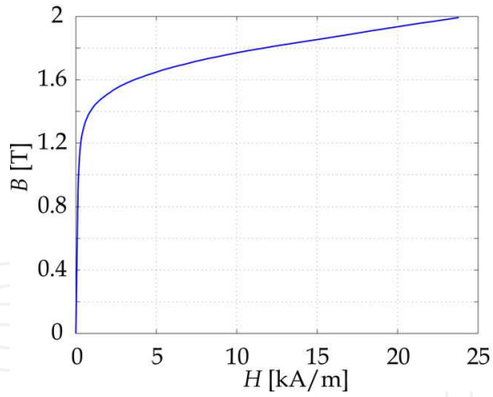

Fig. 3. *B-H* characteristic for laminated ferromagnetic material 330-35-A5

The Poisson's equation (7) is solved numerically using the two dimensional FEM. The stator and rotor are constructed of laminated steel sheets – lamination thickness is 0.35 mm. Ferromagnetic material 330-35-A5, whose magnetization characteristic is shown in Fig. 3 is used. The discretization of the model is shown in Fig. 4a), where standard triangular elements are applied. The non-linear solution of the magnetic vector potential (7) is computed by a conjugate gradient and the Newton-Raphson method. During the analysis of errors, adaptive mesh refinement is applied until the solution error is smaller than a predefined value. Note that the initial mesh is composed of 9973 nodes and 19824 elements, whereas 16442 nodes and 32762 elements are used for the refined mesh. In Fig. 4b) the refined mesh is shown for the air gap region. Example of the magnetic field distribution is shown in Fig. 5. The radial force is computed by Maxwell's stress tensor method (8), where $\boldsymbol{\sigma}$ is Maxwell's stress tensor, $\mathbf{n}$ is the unit vector normal to the integration surface S and $\mathbf{B}$ is the magnetic flux density. The integration is performed over a contour placed along a middle layer of the three-layer mesh in the air gap, as it is shown in Fig. 4b).

$$\mathbf{F} = \oint_S \boldsymbol{\sigma}\, dS = \int_S \left(\tfrac{1}{\mu_0}(\mathbf{B} \bullet \mathbf{n})\mathbf{B} - \tfrac{1}{2\mu_0}\mathbf{B}^2\mathbf{n} \right) dS \tag{8}$$

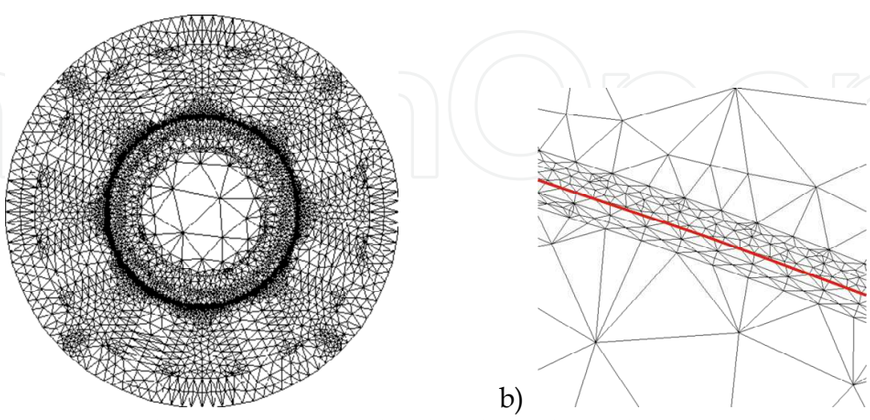

a) b)

Fig. 4. Discretization of the model (a), and refined mesh in the air gap with integration contour for radial force computation (b)

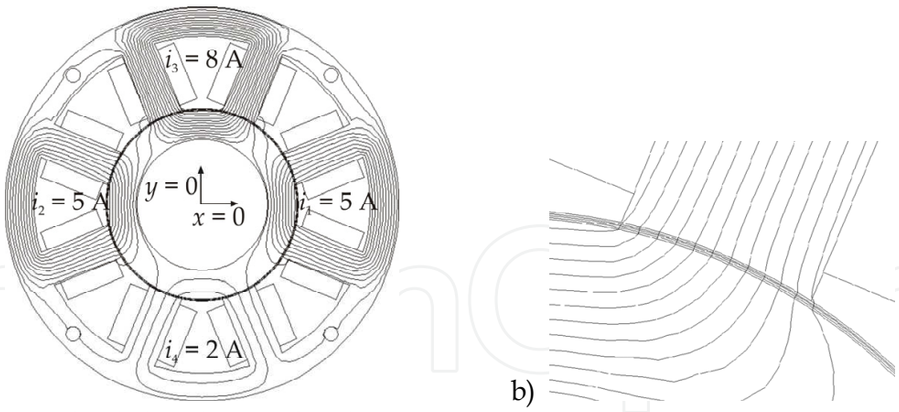

Fig. 5. Magnetic field distribution for the case i_x = 0 A, i_y = 3 A, I_0 = 5 A, and x = y = 0 mm; equipotential plot for the whole geometry (a), and in the air gap and the pole (b)

2.3 Impact of magnetic non-linearities on radial force characteristic

The flux density plot and the equipotential plot is given in Figs. 5 and 6 for a heavy load condition in the y axis (i_x = 0 A, i_y = 3 A) at the rotor central position (x = y = 0). Note that for this case only the radial force in the y axis is generated, whereas the component in the x axis is zero. In Fig. 6 the iron core saturation in the region of the upper electromagnet is observed; an average value of the flux density in the iron core is 1.31 T, whereas at the corners the maximum value of even 1.86 T is reached. However, value of the flux density in the air gap of the upper electromagnet is 1.09 T, as it is marked in Fig. 6. Due to the iron core saturation in the upper electromagnet the radial force generated by a pair of electromagnets in the y axis is reduced. Moreover, the flux lines of the upper electromagnet also link with all other electromagnets, as it is shown in Figs. 5 and 6. Due to these magnetic cross-couplings the asymmetrical air gap flux density is generated in both electromagnets in the x axis, i.e. 0.67 T and 0.70 T (Figure 6). Consequently, electromagnets in the x axis generate a negative radial force component in the y axis, as it is shown by the vector analysis in Fig. 6. In such way, the resultant radial force in the y axis is additionally reduced.

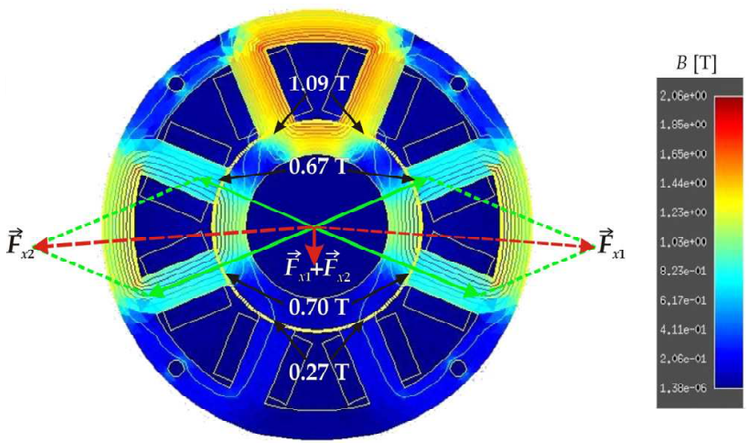

Fig. 6. Magnetic field distribution for the case i_x = 0 A, i_y = 3 A, I_0 = 5 A, and x = y = 0 mm with air gap values of the flux density and vector analysis of a radial force of a pair of electromagnets in the x axis

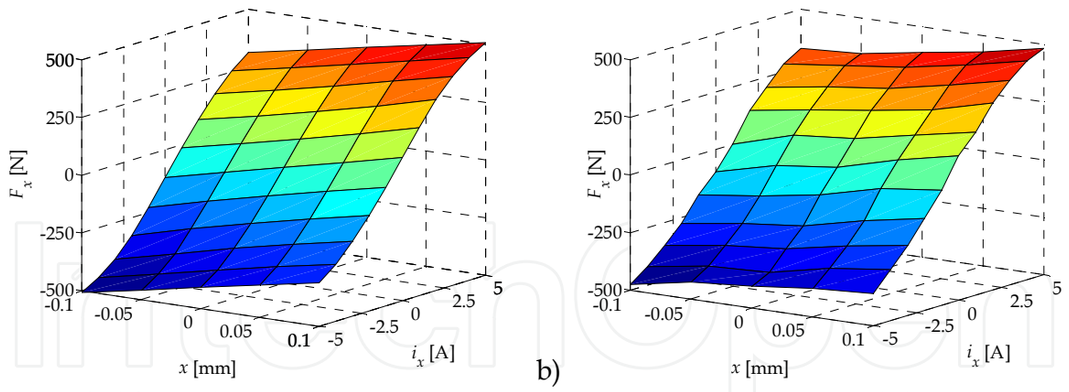

a) b)

Fig. 7. Radial force characteristic $F_x(i_x,x)$: FEM-computed (a), and measured (b)

The radial force characteristic $F_x(i_x,i_y,x,y)$ has been calculated over the entire operating range ($i_x \in$ [-5 A, 5 A], $i_y \in$ [-5 A, 5 A], $x \in$ [-0.1 mm, 0.1 mm], $y \in$ [-0.1 mm, 0.1 mm]). The radial force characteristic $F_x(i_x,x)$ is shown in Fig. 7. A good agreement is obtained between the FEM-computed and measured characteristic. Note that the air gap has been increased in FEM computations from 0.4 to 0.45 mm because the magnetic air gap is larger than the geometric one due to the manufacturing process of the rotor steel sheets. The increase of 0.05 mm in the air gap can be compared with the findings in (Antila et al., 1998). Furthermore, the radial force characteristic $F_x(i_x,x)$ obtained by (1) and (2) are shown in Fig. 8 for the discussed radial AMB. Through the comparison between the FEM-computed and analytical results obtained by a non-linear equation (1) (Figs. 7a and 8a), the considerable radial force reduction is determined. However, in the vicinity of the nominal operating point, the radial force characteristic is surprisingly linear, which is verified through the comparison among the FEM-computed and analytical results obtained by a linearized equation (2) (Figs. 7a and 8b). As it has been already mentioned, the radial force is reduced due to the impact of magnetic non-linearities and cross-coupling effects, especially near the operating range margin ($|i_x| > 2$ A, $|x| > 0.05$ mm), which is reached in the cases of a heavy load unbalanced operation. A more detailed analysis is performed in the section 4 through evaluation of variations of the current gain h_x and position stiffness c_x over the entire operating range.

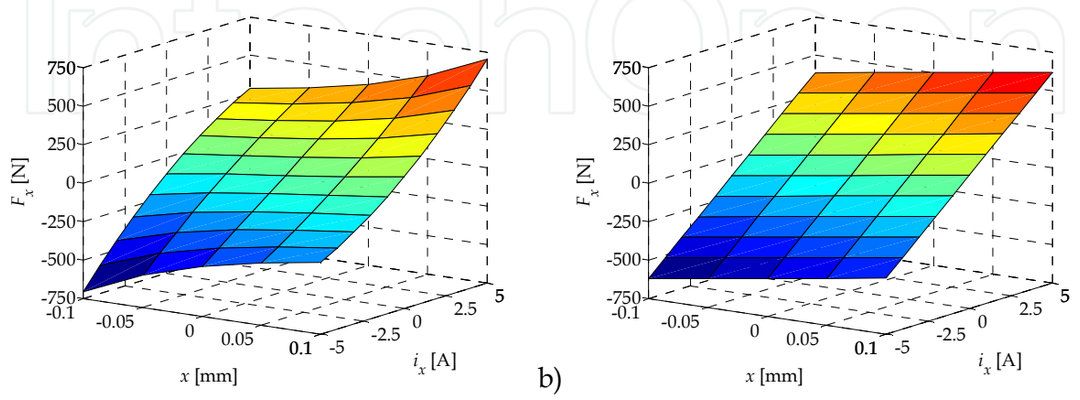

a) b)

Fig. 8. Radial force characteristic $F_x(i_x,x)$: obtained by non-linear equation (1) – (a), and by linearized equation (2) – (b)

3. Design of Radial Active Magnetic Bearings by DE and the FEM

The goal is to design a radial AMB whose radial force characteristic is linear as much as possible over the entire operating range. An experimental radial AMB, shown in Fig. 9 (Polajžer, 2002), is considered for the initial design.
In the author's opinion, DE in combination with the FEM-based analysis is at present still one of the most powerful tools for optimization of such a problem class, where the dependency of the objective function on the design parameters is unknown. According to (Pahner et al., 1998), for optimization of electromagnetic devices in combination with the FEM, DE converges faster and is more stable when compared to other stochastic direct search algorithms such as simulated annealing and self-adaptive evolution strategies. In this work a DE/FEM-based design procedure for radial AMBs is applied, similar to the procedure proposed in our earlier work (Polajžer et al., 2008).

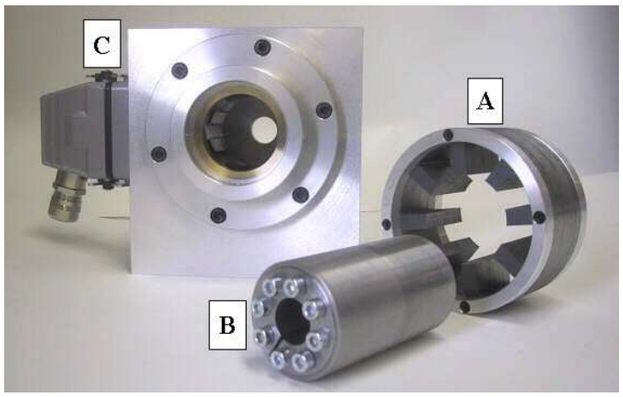

Fig. 9. Experimental radial AMB – initial design: A – stator, B – rotor, C – housing

3.1 Objective function and design parameters

The objective function should be formulated in such a way, that contradictory partial aims are avoided. Otherwise it is possible for the algorithm to stick in a local minimum. This can be prevented by choosing appropriate constraints for the optimization problem. As it is mentioned earlier, the aim is to linearize the radial force characteristic of AMBs over the entire operating range. The non-linearity of a radial force characteristic $F_x(i_x,i_y,x,y)$ is described by the current gain $h_x = \partial F_x/\partial i_x$ and position stiffness $c_x = \partial F_x/\partial x$, which are approximated with differential quotients between two points of the numerically expressed function $F_x(i_x,i_y,x,y)$. The aim of the optimization is thus formulated as a minimization of variations of the linearized AMB model parameters.
The objective function q and penalties p_1, p_2 are found empirically and are defined by (9)–(11). The discussed parameter variations are determined by differences between the nominal and maximal parameter values $\Delta h_x = (h_{x,\mathrm{nom}} - h_{x,\mathrm{max}})$ and $\Delta c_x = (c_{x,\mathrm{nom}} - c_{x,\mathrm{max}})$. The nominal parameter values refer to the nominal operating point where the rotor is in the central position ($x = y = 0$), while both control currents equal zero ($i_x = i_y = 0$). The maximal parameter values refer to the maximal rotor eccentricity ($x = y = E_{\mathrm{max}}$) and maximal control currents ($i_x = i_y = I_0$), which is expected for a heavy load unbalanced operation. Note that the differences $\Delta h_{x0} := (h_{x0,\mathrm{nom}} - h_{x0,\mathrm{max}})$ and $\Delta c_{x0} := (c_{x0,\mathrm{nom}} - c_{x0,\mathrm{max}})$ are defined for the initial AMB design.

$$q = 0.8\frac{\left|\Delta h_y\right|}{\Delta h_{y0}} + 0.2\frac{\left|\Delta c_y\right|}{\Delta c_{y0}} + p_1 + p_2 \tag{9}$$

$$p_1 = 0.8\frac{\left|\Delta h_y\right|}{\Delta h_{y0}} \quad \text{if} \quad \left|\Delta h_y\right| > 1.1\,\Delta h_{y0} \tag{10}$$

$$p_2 = 0.2\frac{\left|\Delta c_y\right|}{\Delta c_{y0}} \quad \text{if} \quad \left|\Delta c_y\right| > 1.1\,\Delta c_{y0} \tag{11}$$

The design parameters (x_1, x_2, x_3, x_4) are the rotor yoke width w_{ry}, stator yoke width w_{sy}, pole width w_p (all shown in Fig. 10) and axial length of the bearing l, respectively. The design constraints are fixed mainly by the mounting conditions, which are given by the shaft radius r_{sh} = 17.5 mm and stator outer radius r_s = 52.8 mm (Fig. 10). Two additional constraints are given by the nominal air gap δ_0 = 0.45 mm and the bias current I_0 = 5 A in order to achieve the maximum force slew rate $|dF/dt|_{\max} = 5{\cdot}10^6$ N/s. Furthermore, the maximum eccentricity of the rotor $E_{\max}$ = 0.1 mm is determined in order to prevent the rotor touchdown.

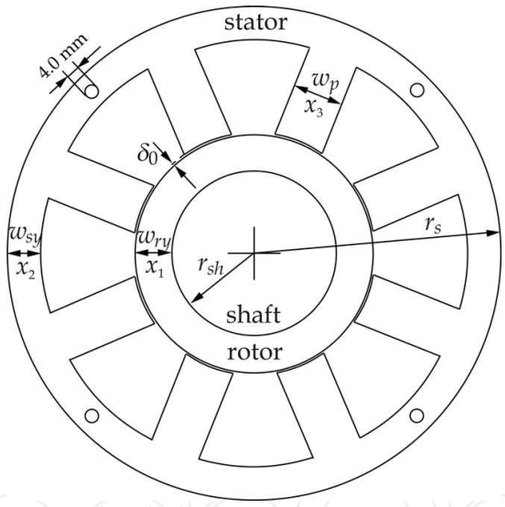

Fig. 10. Geometry of the discussed radial AMB – design parameters are denoted by x_1, x_2, x_3

3.2 Optimization procedure

Optimization of the discussed radial AMBs has been carried out in a special programming environment tuned for FEM-based numerical optimizations (Pahner et al., 1998). The procedure is described by the following steps:

- **Step 1)** The geometry of the initial AMB is described parametrically.
- **Step 2)** The new values for the design parameters are determined by the DE (Price et al., 2005), where strategy "DE/best/1/exp" is used with the population size NP = 25, the DE step size F = 0.5 and for the crossover probability constant CR = 0.75.
- **Step 3)** The geometry, the materials, the current densities, and the boundary conditions are defined. The procedure continues with **Step 2)** if the parameters of the bearing are outside the design constraints.

- **Step 4)** The radial force is computed by the FEM, as it is described in the previous section. Computations are performed for eight different cases: near the nominal operating point for $i_x = 0 \pm 0.1 I_0$ and $x = 0 \pm 0.1 E_{max}$, as well as near the maximal operating point for $i_x = 0.9 I_0 \pm 0.1 I_0$ and $x = E_{max} \pm 0.1 E_{max}$. Note that the control current i_y and the rotor position in the y axis are both zero during these computations.
- **Step 5)** The current gain values $h_{x,nom}$ and $h_{x,max}$, as well as the position stiffness values $c_{x,nom}$ and $c_{x,max}$ are calculated with differential quotients, whereas values of the radial force are obtained from **Step 4)**.
- **Step 6)** The value of the objective function (9) is calculated. The optimization proceeds with **Step 2)** until a minimal optimization parameter variation step or a maximal number of evolutionary iterations are reached.

3.3 Results of the optimization

The objective function has been minimized from 1 to even 0.46, while the minimal value has been reached after 41 iterations. The data and parameters for the initial – non-optimized radial AMB and for the optimized radial AMB are given in Table 1. All design parameters are rounded off to one tenth of a millimetre. Nominal values for the current gain and position stiffness, i.e. at the nominal operating point ($i_x = 0$, $x = 0$), as well as the mass of the rotor of the optimized bearing are, indeed, slightly lower. Consequently, the controller settings need to be recalculated for the new nominal parameter values. In such way the closed-loop system dynamics is not changed. Furthermore, the maximal force at the rotor central position ($x = y = 0$) is increased within the optimized design.

Parameter	Non-optimized	Optimized
Rotor yoke width w_{ry} [mm]	7.7	5.1
Stator yoke width w_{sy} [mm]	7.8	9.1
Pole width w_p [mm]	9.4	5.3
Axial length l [mm]	38	45.6
Current gain $h_{x,nom}$ [N/A]	100.8	95.6
Position stiffness $c_{x,nom}$ [N/mm]	1161	967
Maximal force $F_{x,max}$ [N]	411	435
Rotor mass m [kg]	0.596	0.576

Table 1. Data and parameters for the non-optimized and optimized radial AMB

4. Evaluation of static and dynamic properties of non-optimized and optimized radial AMB

4.1 Current gain and position stiffness characteristics

The current gain and position stiffness characteristics $h_x(i_x,i_y,x,y)$ and $i_x(i_x,i_y,x,y)$ are determined by approximations with differential quotients over the entire operating range ($i_x \in$ [-5 A, 5 A], $i_y \in$ [-5 A, 5 A], $x \in$ [-0.1 mm, 0.1 mm], $y \in$ [-0.1 mm, 0.1 mm]). The obtained results are shown in Figs. 11–14, where characteristics are normalized to the nominal parameter values, which are defined at the nominal operating point ($x = y = 0$, $i_x = i_y = 0$) and are given in Table 1. In Figs. 11 and 13 the current gain and position stiffness characteristics are shown for the non-optimized radial AMB. The current gain and position stiffness characteristics for the optimized radial AMB are shown in Figs. 12 and 14.

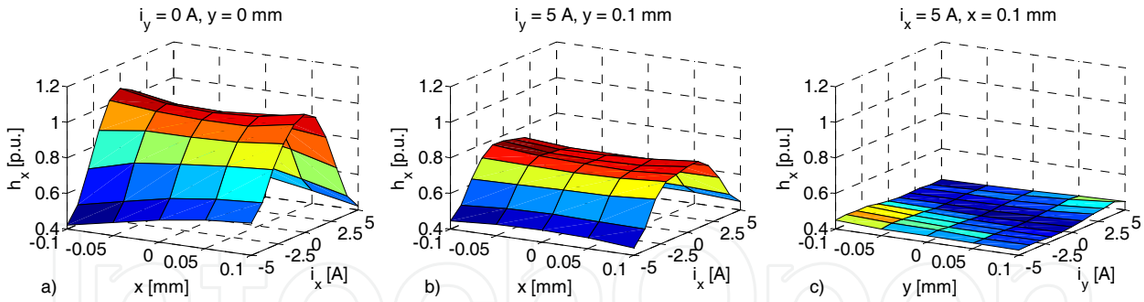

Fig. 11. Current gain characteristic $h_x(i_x,i_y,x,y)$ normalized to the nominal value 100.8 N/A – non-optimized AMB

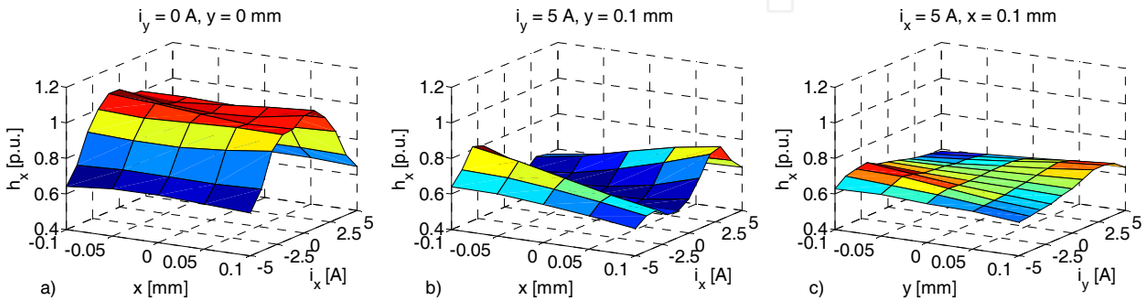

Fig. 12. Current gain characteristic $h_x(i_x,i_y,x,y)$ normalized to the nominal value 95.6 N/A – optimized AMB

In order to evaluate the obtained results, maximal and average variations are determined over the entire operating range ($i_x \in$ [-5 A, 5 A], $i_y \in$ [-5 A, 5 A], $x \in$ [-0.1 mm, 0.1 mm], $y \in$ [-0.1 mm, 0.1 mm]), and for the high signal amplitudes ($|i_x| >$ 2 A, $|i_y| >$ 2 A, $|x| >$ 0.05 mm, $|y| >$ 0.05 mm). Note that all variations are given relatively with respect to the nominal parameter values.

Let us first observe maximal variations of the current gain and the position stiffness. The obtained maximal variation of the current gain is 59% for the non-optimized design and 46% for the optimized design, whereas the obtained maximal variation of the position stiffness is 40% for the non-optimized design and 32% for the optimized design. Average parameter variations are determined next. When observed over the entire operating range, average variation of the current gain is 27% for the non-optimized design and 20% for the optimized design, whereas average variation of the position stiffness is 14% for the non-optimized design and 13% for the optimized design. However, when the margin of the operating range is observed (high signal case), average variation of the current gain is 43% for the non-optimized design and 28% for the optimized design, whereas average variation of the position stiffness is 21% for the non-optimized design and 13% for the optimized design.

Based on the performed evaluation of the obtained results, it can be concluded that the impact of magnetic non-linearities on variations of the linearized AMB model parameters is considerably lower for the optimized AMB, particularly for high signal amplitudes. However, the impact of magnetic cross-couplings slightly increases. Furthermore, normalized values of the current gain and position stiffness are higher for the optimized AMB. Consequently higher load forces are possible for the optimized AMB, as it is shown in the following section.

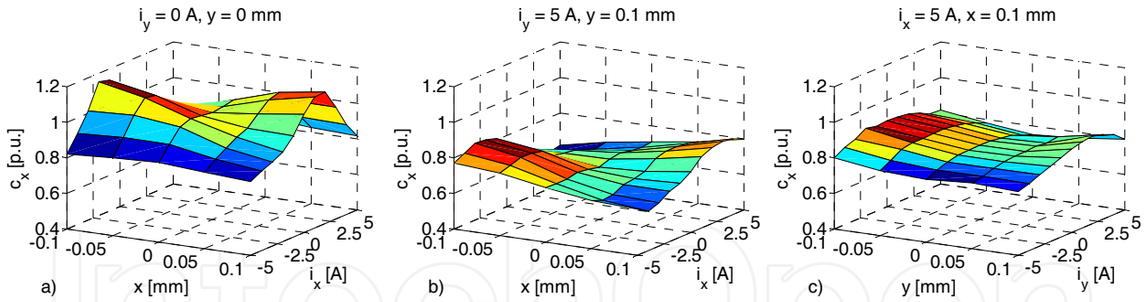

Fig. 13. Position stiffness characteristic $c_x(i_x,i_y,x,y)$ normalized to the nominal value 1161 N/mm – non-optimized AMB

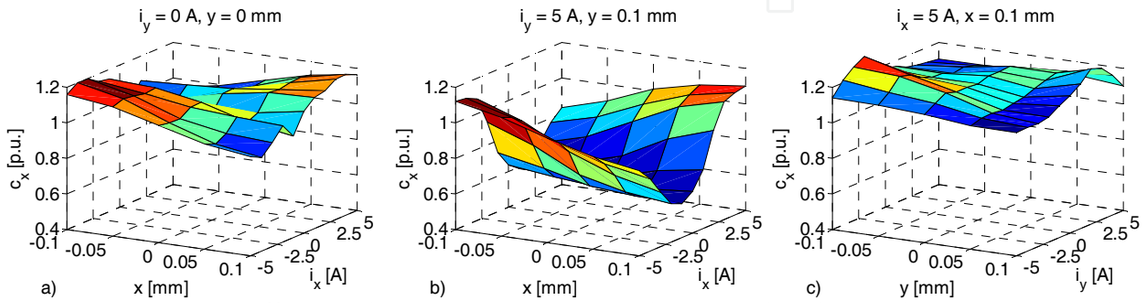

Fig. 14. Position stiffness characteristic $c_x(i_x,i_y,x,y)$ normalized to the nominal value 967 N/mm – optimized AMB

4.2 Dynamic behaviour of a closed-loop controlled system

In order to evaluate the robustness of the closed-loop controlled system, two radial AMBs that control the unbalanced rigid shaft are modeled. A dynamic model is tested for the non-optimized and for the optimized radial AMBs, where calculated radial force characteristics $F_x(i_x,i_y,x,y)$ and $F_y(i_x,i_y,x,y)$ are incorporated. The AMB coils are supplied with ideal current sources, whereas the impact of electromotive forces is not taken into account. The structure of the closed-loop system used in numerical simulations is shown in Fig. 15, where $\mathbf{i} = [i_x, i_y]^T$, $\mathbf{F} = [F_x, F_y]^T$ and $\mathbf{y} = [x, y]^T$ denote current, force and position vectors, respectively. The reference position vector is denoted as $\mathbf{y}_r = [x_r, y_r]^T$, whereas $\mathbf{d} = [F_{dx}, F_{dy} + mg]^T$ is the disturbance vector. In order to evaluate the impact of non-linearities of the radial force characteristic on the closed-loop system, a decentralized control feedback is employed. Position control loops are realized by two independent PID controllers in the x and y axis.

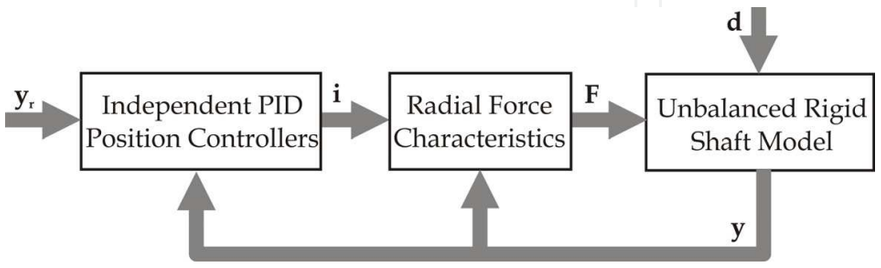

Fig. 15. Structure of the closed-loop AMB system

Responses for the rotor position in the x and y axis and for the control currents i_x and i_y are calculated with Matlab/Simulink®. Fig. 16 shows results of the no rotation test, where the reference rotor position and the disturbance forces are changed in the following sequence: $F_{dy}(0.1) = 250$ N, $y_r(0.3) = -0.09$ mm, $F_{dx}(0.5) = 100$ N and $x_r(0.7) = -0.1$ mm. In the obtained results, it can be noticed that for the case of a reference position change, a considerably higher closed-loop damping is achieved within optimized AMBs, whereas for the heavy load case considerably higher closed-loop stiffness is achieved again within the optimized AMBs. The impact of cross-coupling effects can also be noticed, since changes in the x axis variables are reflected in the y axis variables. Furthermore, from the results shown in Fig. 16, it can be concluded that the control current is much higher for the non-optimized AMBs. Consequently, an operation with the considerably higher load forces can be achieved within the optimized AMBs.

These conclusions are completely confirmed with the results of a simulation unbalance test, which are shown in Figs. 17 and 18. A rotation with 6000 rpm of a highly unbalanced rigid shaft is simulated. Consequently, the unbalanced responses are obtained, which is shown by trajectories of the rotor position and control currents. The trajectories for the unbalanced no load condition are shown together with the trajectories during the 180 N load impact in the y axis. From the obtained results it can be noticed that during the no load condition the rotor eccentricity is slightly larger for the optimized AMBs. Note that this is mostly due to the lower current gain and position stiffness in the linear region. However, during the heavy load operation a current limit is reached (5 A) in the case of the non-optimized AMBs (Fig. 17), whereas the rotor eccentricity is critical (>0.1 mm). On the contrary, the unbalanced response of the optimized design is much less severe, which is mostly due to lower variations of the current gain and position stiffness. The rotor eccentricity stays within the safety boundaries (±0.1 mm), as it is shown in Fig. 18, whereas for the same load condition considerably lower control currents are applied.

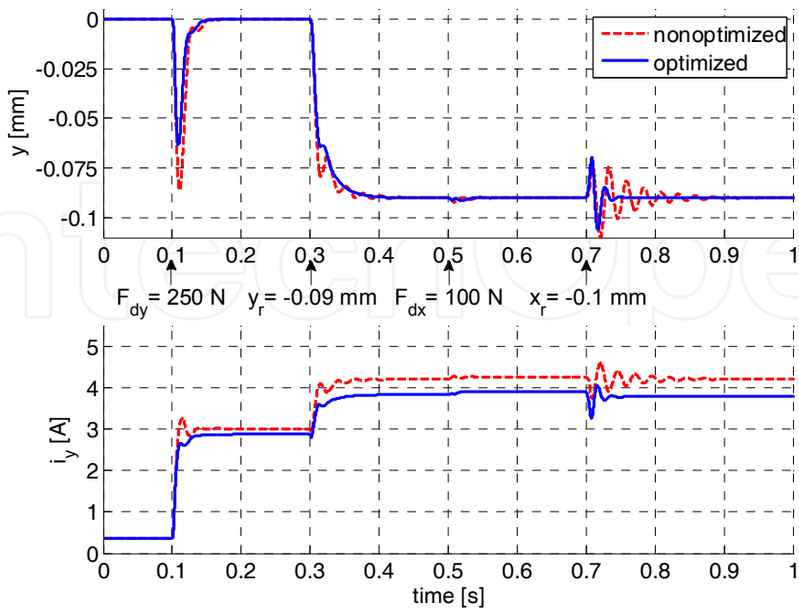

Fig. 16. Simulation-based time responses of the non-optimized and optimized radial AMBs

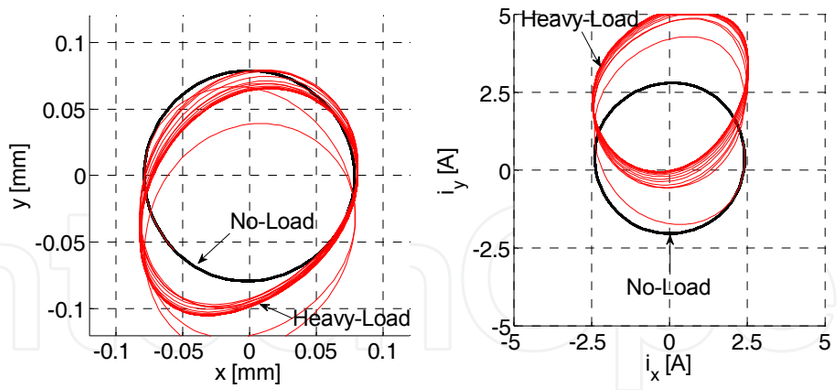

Fig. 17. Simulation-based unbalance responses for rotation test at 6000 rmp and 180 N load impact in the *y* axis – non-optimized AMBs

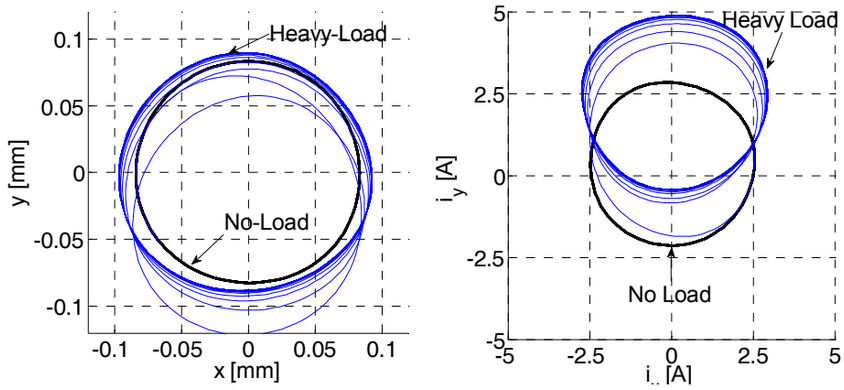

Fig. 18. Simulation-based unbalance responses for rotation test at 6000 rmp and 180 N load impact in the *y* axis – optimized AMBs

5. Conclusion

This work deals with non-linearities of radial force characteristic of AMBs. A linearized AMB model for one axis is presented first. It is used to define the current gain and position stiffness, parameters that are used for calculation of the controller settings. Next, FEM-based computations of the radial force are described. Based on the obtained results, a considerable radial force reduction is determined. It is caused by the magnetic non-linearities and cross-coupling effects. Therefore, the optimization of a radial AMB is proposed, where the aim is to find a such design, where a radial force characteristic is linear as much as possible over the entire operating range. A combination of differential evolution and FEM-based analysis is used, whereas the objective function is minimized by even 54%. Static and dynamic properties of the non-optimized and optimized AMB are evaluated in final section. The results presented here show that considerably lower variations of the current gain and position stiffness are achieved for the optimized AMB over the entire operating range, especially on its margins that are reached during heavy load unbalanced operation. Furthermore, a closed-loop damping and stiffness of an overall system are considerably higher with the optimized AMBs. Moreover, the operation with the higher load forces is also expected for the optimized radial AMB.

6. References

Antila, M., Lantto, E. & Arkkio, A. (1998). Determination of forces and linearized parameters of radial active magnetic bearings by finite element technique. *IEEE Transactions on Magnetics*. Vol. 34, No. 3, pp. 684–694.

Bleuer, H., Gähler, C., Herzog, R., Larsonneur, R., Mizuno, T., Siegwart, R., Woo, S.-J., (1994). Application of digital signal processors for industrial magnetic bearings. *IEEE Transactions on control systems technology.* Vol. 2, No. 4, pp. 278-289.

Carlson-Skalak, S., Maslen, E., & Teng, Y. (1999). Magnetic bearings actuator design using genetic alghoritms. *Journal of Engineering Design*. Vol. 10, No. 2, pp. 143–164.

Hameyer, K. & Belmans, R. (1999). *Numerical modelling and design of electrical machines and devices.* WIT Press, Suthampton.

ISMB12, (2010). The Twelfth International Symposium on Magnetic Bearings, Wuhan, China, http://ismb12.meeting.whut.edu.cn/

Knospe, C. R. & Collins, E. G. (1999). Introduction to the special issue on magnetic bearing control. *IEEE Transactions on control systems technology.* Vol. 4, No. 5, pp. 481–483.

Larsonneur, R. (1994). *Design and control of active magnetic bearing systems for high speed rotation,* Ph.D. dissertation, ETH Zürich.

Maslen, E. H. (1997). Radial bearing design, in *Short Course on Magnetic Bearings*, Lecture 7, Alexandria, Virginia.

Meeker, D. C. (1996). *Optimal solutions to the inverse problem in quadratic magnetic actuators,* Ph.D. dissertation, School of Engineering and Applied Science, University of Virginia.

Pahner, U., Mertens, R., DeGersem, H., Belmans, R. & Hameyer, K. (1998). A parametric finite element environment tuned for numerical optimization. *IEEE Transactions on Magnetics*. Vol. 34, No. 5, pp. 2936–2939.

Polajžer, B. (2002). *Design and analysis of an active magnetic bearing experimental system,* Ph.D. dissertation, University of Maribor, Faculty of Electrical Engineering and Computer Science, Maribor.

Polajžer, B., Štumberger, G., Ritonja, J. & Dolinar, D. (2008). Variations of active magnetic bearings linearized model parameters analyzed by finite element computation. *IEEE Transactions on Magnetics.* Vol. 44, No. 6, pp. 1534–1537.

Price, K., Storn, R., & Lampinen, J. (2005). *Differential evolution: a practical approach to global optimization*. Springer-Verlag: Berlin Heidelberg.

Rosner, C. H. (2001). Superconductivity: star technology for the 21st century. *IEEE Transactions on applied superconductivity.* Vol. 11, No. 1, pp. 39–48.

Schweitzer, G., Bleuler, H. & Traxler A. (1994). *Active magnetic bearings: Basics, properties and applications of active magnetic bearings*, Vdf Hochschulverlag AG an der ETH Zürich.

Štumberger, G., Dolinar, D., Pahner, U. & Hameyer, K. (2000). Optimization of radial active magnetic bearings using the finite element technique and the differential evolution algorithm. *IEEE Transactions on Magnetics.* Vol. 36, No. 4, pp. 1009–1013.

Magnetic Bearings, Theory and Applications

Edited by Bostjan Polajzer

ISBN 978-953-307-148-0

Hard cover, 132 pages

Publisher Sciyo

Published online 06, October, 2010

Published in print edition October, 2010

The term magnetic bearings refers to devices that provide stable suspension of a rotor. Because of the contact-less motion of the rotor, magnetic bearings offer many advantages for various applications. Commercial applications include compressors, centrifuges, high-speed turbines, energy-storage flywheels, high-precision machine tools, etc. Magnetic bearings are a typical mechatronic product. Thus, a great deal of knowledge is necessary for its design, construction and operation. This book is a collection of writings on magnetic bearings, presented in fragments and divided into six chapters. Hopefully, this book will provide not only an introduction but also a number of key aspects of magnetic bearings theory and applications. Last but not least, the presented content is free, which is of great importance, especially for young researcher and engineers in the field.

InTech Europe
University Campus STeP Ri
Slavka Krautzeka 83/A
51000 Rijeka, Croatia
Phone: +385 (51) 770 447
Fax: +385 (51) 686 166
www.intechopen.com

InTech China
Unit 405, Office Block, Hotel Equatorial Shanghai
No.65, Yan An Road (West), Shanghai, 200040, China
中国上海市延安西路65号上海国际贵都大饭店办公楼405单元
Phone: +86-21-62489820
Fax: +86-21-62489821

IntechOpen